CHAPTER 10

AUGER ELECTRON SPECTROSCOPY

Richard P. Gunawardane and Christopher R. Arumainayagam
Department of Chemistry, Wellesley College, Wellesley, MA 02481, U.S.A.

10.1 INTRODUCTION

Auger electron spectroscopy (AES) is a nondestructive core-level electron spectroscopy for semi-quantitative determination of the elemental composition of surfaces, thin films, and interfaces. The popularity of this ultrahigh vacuum technique may be attributed to high surface sensitivity (an analysis depth of less than 100 Å) and a relatively low detection limit (~0.1 atomic percent). In addition to having an elemental coverage from lithium to uranium and beyond, AES has the ability to distinguish between two elements that are close to each other in the periodic table. In addition, AES has an atomic number-dependent sensitivity that varies at most by one order of magnitude. AES chemical shifts and line shapes can also yield bonding (chemical state) information, albeit with less precision than is possible with X-ray photoelectron spectroscopy (XPS) (Chapter 11), another core-level electron spectroscopy. Auger electron spectroscopy has a depth resolution of 5–25 Å, and can be used, with simultaneous ion sputtering, for depth profiling. With a lateral resolution (<100 Å) that is significantly better than that of XPS, *scanning Auger microscopy* (SAM) can be used effectively for imaging nanoscale structures and to produce two-dimensional maps of surface elemental composition. Survey Auger spectra typically take less than five minutes, providing for rapid data acquisition. Although somewhat sophisticated and expensive, Auger instrumentation is relatively simple to use and is readily available from many different commercial sources. The reasons enumerated above explain why Auger electron spectroscopy has become perhaps the most widely used surface analytical technique.

Recent developments in AES have expanded the scope of this technique beyond the probing of surface elemental composition. For example, spin polari-zation of Auger electrons can be used to study magnetized solid surfaces [1]. Moreover, results of resonant Auger electron spectroscopy experiments provide information relevant to femtosecond charge transfer dynamics [2]. Auger electron diffraction can also be used to determine surface

structure [3]. Finally, results of recent experiments have demonstrated that angle-resolved Auger electron spectroscopy can provide a means to study excitation processes in solids [4].

The Auger process is a three-electron process. When a beam of electrons, typically with an energy range of 3–20 keV, strikes a solid atom, a core-level (inner) electron is ejected producing a singly ionized excited atom. An outer level electron can fill the resulting vacancy in the core level. Following this radiationless transition, the excess energy of the resulting excited state ion may be removed by emitting either (i) an X-ray (the basis for X-ray fluorescence (XRF)/electron microprobe (EMP) analysis) or (ii) another electron from the atom. The emitted electrons in process (ii) are called *Auger electrons*, after Pierre Auger, who discovered this process in the 1920s [5]. Although Lise Meitner independently discovered the effect around the same time [6], she is given very little recognition in the literature. While the emission of X-rays (process (i)) produces singly ionized atoms, the emission of Auger electrons (process (ii)) results in doubly ionized atoms.

Because Auger is a three-electron process, hydrogen and helium cannot be detected by this technique. Although Li has three electrons, an *isolated ground state* Li atom does not yield Auger peaks because the atom has only two energy levels that contain electrons. Auger peaks, however, have been detected from multiply excited Li atoms [7]. The presence of electrons in the valence band of *solid* Li also allows for Auger transitions of the type KVV.

The surface sensitivity of AES is due to the short mean free path of the relatively low energy Auger electrons. Although atomic excitations can take place to a depth of ~10,000 Å below the surface, the Auger electrons from only the uppermost atomic layers, down to a depth of ~100 Å, are ejected from the specimen without undergoing any energy loss. In contrast, electron microprobe analysis, involving the detection of X-ray photons, is more of a *bulk*, rather than a *surface*, analysis tool (Figure 10.1).

Because of the very short lifetime of the electronic states associated with the Auger process, the Auger peaks are relatively wide (typically 1–2 eV), consistent with Heisenberg's uncertainty principle.

The kinetic energies of the Auger electrons are characteristic of each emitting atom. Thus, the measurement of the kinetic energies of Auger electrons can be used to identify the elements present on the surface of the sample. Because the kinetic energies of Auger electrons depend on the binding energies of the electron levels involved in the Auger process, the shifts in these kinetic energies can, in principle, provide useful information on the oxidation states and bonding environment of the surface atoms. In addition to the above qualitative analysis, quantitative information may also be determined from the intensities of the Auger peaks.

A *direct* Auger spectrum is represented as a plot of the number of electrons detected as a function of electron kinetic energy. However, to make the small Auger peaks more prominent, often AES spectra are displayed as the first derivative of the number of electrons emitted as a function of electron

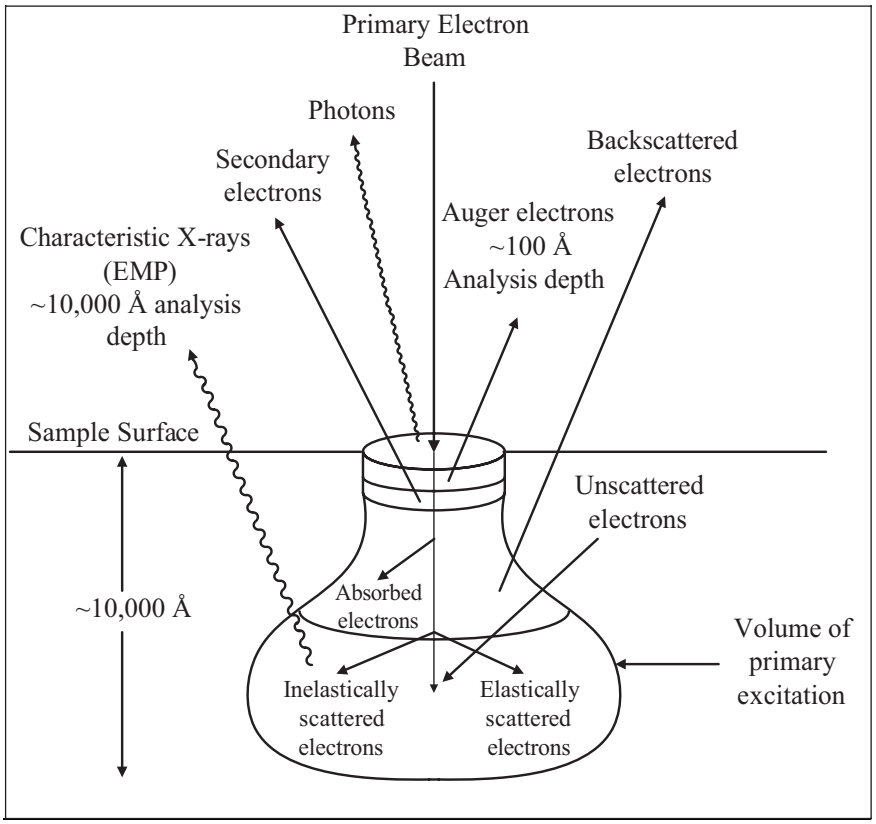

Figure 10.1 Schematic diagram showing the various locations and outcomes of electron-solid interactions (a composite diagram based on various sources) [8, 9].

kinetic energy. The derivative form of the Auger spectrum enhances the Auger peaks and suppresses the background arising from the secondary and backscattered electrons.

The AES analysis is carried out in an *ultrahigh vacuum* (UHV) chamber in which a pressure of ~10^{-9} torr or below is continuously maintained. High vacuum is necessary to allow uninterrupted passage of the electron beam and ultrahigh vacuum is necessary to avoid contamination of the surface by atmospheric gases during analysis.

The goal of this chapter is to provide a detailed introduction to Auger electron spectroscopy. Topics covered emphasize physical principles, experimental techniques and procedures, research and industrial applications, and new developments in Auger electron spectroscopy. For a more detailed treatment of the technique and its applications, the reader is referred to a 900-page comprehensive treatise on Auger and X-ray photoelectron spectroscopy published recently [10]. A less extensive text devoted to the above two techniques was published in 2003 [11].

10.2 HISTORICAL PERSPECTIVE

The historical developments of Auger electron spectroscopy have been comprehensively reviewed [12]. Here we provide a brief synopsis. The name "Auger electron spectroscopy" is derived from the effect reported in 1923 by Pierre Auger, a French physicist. Three decades passed before J.J. Lander first applied this phenomenon to solids in 1953 [13]. L.A. Harris demonstrated in 1968 the utility of taking derivatives for plotting AES spectra [14]. Initially, the retarding field analyzer (RFA) used in low energy electron diffraction (LEED) experiments was modified by many research groups to obtain Auger spectra [15]. In 1969 Palmberg and coworkers developed the cylindrical mirror analyzer (CMA) for detecting Auger electrons [16]. The first commercial Auger electron spectrometers also became available in 1969. Scanning Auger microscopy (SAM) was first demonstrated in 1971 by MacDonald and Waldrop [17] and later developed extensively by Prutton and coworkers [18, 19]. Auger depth profiling with noble gas ion sputtering was first demonstrated by Palmberg in 1972 [20]. AES instrumentation has undergone considerable improvement over the years leading to automation with computer control and use of modern software for sophisticated data analysis.

10.3 BASIC PRINCIPLES OF AES

10.3.1 X-Ray Notation

In Auger electron spectroscopy, electron energy states are denoted by using X-ray notation. Because removing an electron from a complete shell is equivalent to placing a single electron in an empty shell, X-ray spectra are similar to one-electron alkali atom spectra. Hence, we first examine the *fine structure* in the optical spectra of alkali atoms. The fine structure, the splitting of lines (with the exception of those due to s-state electrons) in the spectra of alkali atoms into doublets, is due to *spin-orbit coupling*, the interaction of the spin magnetic moment with the magnetic field arising from the orbital angular momentum. Spin-orbit coupling splits non-s energy *terms* in alkali atoms into two *levels*.

We now discuss the terminology used for electronic energy *levels* for light atoms, for which Russell-Saunders coupling (*also called L-S coupling*) is a valid approximation. In the general case, each level is specified by the principle quantum number (n) and a level symbol ($^{2S+1}L_J$). In this symbol, S is the total electronic *spin angular* momentum quantum number, L is the code for the total electronic *orbital angular* momentum quantum number, and J is the total electronic *angular* momentum quantum number. Because X-ray spectra are similar to one-electron alkali atom spectra, the following simplification is made to yield the *XPS notation.* In addition to the principal

quantum number (n), the energy level can be specified with the orbital angular momentum (ℓ) and the total angular momentum quantum number (j) of a *single* electron. The spin multiplicity $2S+1$ can be ignored because it is always 2 for a one-electron (one-hole) atom since $S = ½$. The total angular momentum of a single electron is obtained by using the Clebsch-Gordon series:

$$j = \ell + s,\ \ \ell + s - 1, ..., \left|\ell - s\right|. \tag{10.1}$$

In the above expression, ℓ is the orbital angular momentum quantum number and s is the spin angular momentum quantum number, which is ½ for all electrons. The general form of the XPS notation is $n\ell_j$.

We illustrate the above discussion with a specific example involving the fine structure of the sodium D line. The excited Na atom electron configuration ($1s^2 2s^2 2p^6 3p$) yields the ^2P term because $L = \ell = 1$ and $S = s = ½$. Using the Clebsch-Gordon series we obtain $J = 1 - ½$ and $1 + ½$, yielding two levels ($^2P_{1/2}$ and $^2P_{3/2}$) for the ^2P term.

The principal quantum number 3 is often omitted. As is often done in X-ray photoelectron spectroscopy, the above two energy levels may be written alternatively as $3p_{1/2}$ and $3p_{3/2}$.

Specifying the energy levels with *Auger notation* involves using the letters K, L, M,… for the principal quantum number 1, 2, 3,… and a subscript that depends on the orbital quantum number (ℓ) and the total angular momentum quantum number (j). For example, the two levels $^2P_{1/2}$ and $^2P_{3/2}$—the energy levels of the excited Na atom—may be written as M_2 and M_3. Note that M_1 is the Auger notation for the energy level of the ground state electron configuration ($1s^2 2s^2 2p^6 3s$) of the Na atom. The level symbol for the ground state electron configuration is $^2S_{½}$ corresponding to the XPS notation of $3s_{½}$. When the energy levels are very close to each other they are not usually resolvable experimentally. These unresolvable energy levels are normally designated with a comma between the subscripts (e.g., $L_{2,3}$ and $M_{4,5}$). We summarize the above discussion in Table 10.1

10.3.2 Auger Transitions

The Auger process for a solid is schematically illustrated in Figure 10.2. The KL_2L_3 Auger transition, illustrated in this diagram, involving ionization, relaxation, and emission, may be visualized as follows:

(1) A core-electron in the atom is removed by the high-energy incident electron creating a vacancy in the K shell and yielding an electronically excited ion (ionization).
(2) An electron from the L_2 level falls down almost immediately in a radiationless transition to fill the vacancy in the K shell (relaxation).

Table 10.1 X-ray notation of electron energy states.

Quantum Numbers			Level Symbol	Auger Notation	XPS Notation
n	ℓ	j			
1	0	1/2	$^2S_{½}$	K	$1s_{1/2}$
2	0	1/2	$^2S_{½}$	L_1	$2s_{1/2}$
2	1	1/2	$^2P_{½}$	L_2	$2p_{1/2}$
2	1	3/2	$^2P_{3/2}$	L_3	$2p_{3/2}$
3	0	1/2	$^2S_{½}$	M_1	$3s_{1/2}$
3	1	1/2	$^2P_{½}$	M_2	$3p_{1/2}$
3	1	3/2	$^2P_{3/2}$	M_3	$3p_{3/2}$
3	2	3/2	$^2D_{3/2}$	M_4	$3d_{3/2}$
3	2	5/2	$^2D_{5/2}$	M_5	$3d_{5/2}$

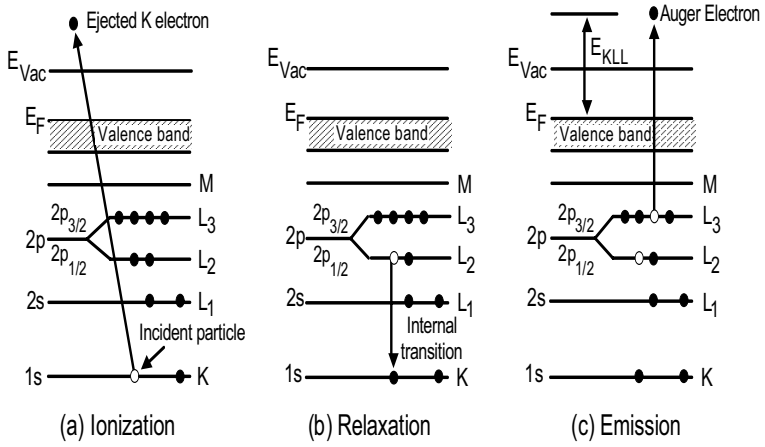

Figure 10.2 Schematic showing the three steps involved in the Auger process. The KL_2L_3 Auger transition is illustrated. The open circles symbolize holes (absence of electrons).

(3) Excess energy of the excited state ion is removed by the ejection of an Auger electron from the L_3 level (emission).

The nomenclature of the Auger transition indicates the energy levels in the order in which they are involved in the whole process. Thus, the transition described above may be designated as KL_2L_3. In the context of Russell-Saunders coupling, there are six KLL transitions corresponding to the three final electron configurations, as shown in Table 10.2.

Table 10.2 KLL Auger transitions corresponding to the different final electron configurations.

Final Electron Configuration	Auger Transition
$2s^0 2p^6$	KL_1L_1
$2s^1 2p^5$	KL_1L_2 KL_1L_3
$2s^2 2p^4$	KL_2L_2 KL_2L_3 KL_3L_3

Although many Auger transitions are available, especially for atoms with high atomic number, most have low probabilities. Some transitions, although energetically allowed, are forbidden due to selection rules. When a valence electron is involved, the letter V is often used (e.g., KLV, KVV, and LMV). The letter C is sometimes used to denote a core level (e.g., CVV). The strongest Auger transitions are of the type ABB (e.g., KLL and LMM). Special transition of the type AAB, commonly termed *Coster-Kronig transitions*, are also very strong.

X-ray emission is a competing process for Auger emission because the energy difference between the core and outer levels can also be released in the form of a characteristic X-ray. The sum of the Auger yield and X-ray emission yield is unity. It has been observed that the probability for X-ray emission is much lower than the Auger emission for the range of energies normally measured in AES [34]. Moreover, for elements with low atomic numbers, the cross-section for the Auger process is much higher than that for emission of X-ray photons.

10.3.3 Kinetic Energies of Auger Electrons

Auger electron spectroscopy involves measurement of the Auger electron's kinetic energies that are characteristic of the elements present in the sample. An uncertainty of 1 to 2 eV in the measurement of the kinetic energy is acceptable for elemental identification. For the purpose of Auger chemical shift analysis, however, the uncertainty in kinetic energy measurements must be reduced to 0.1 to 0.2 eV [21]. Extensive work has been performed to calibrate and standardize Auger electron energies [22–25]. Before the advent of Auger databases, the identification of elements via AES required the computation of Auger electron energies, as summarized below.

The kinetic energy of an Auger electron is the energy difference between the doubly ionized final state and the singly ionized initial state. Because calculating Auger electron energies based on first principles is highly complex, and because errors on the order of ~10 eV are acceptable for most practical purposes, we make several approximations. Let us consider an ABC

Auger transition in which the first electron is ejected creating a hole in the A level, the second electron falls from the B level to the A level, and the third electron (the Auger electron) is ejected from the C level. Let E_A, E_B, and E_C be the binding energies of electrons in A, B, and C levels, respectively, of the neutral atom. The energy released $(E_A - E_B)$ when the second electron falls from level B to level A is transferred to the third electron. Hence, the kinetic energy (E_{ABC}) of this Auger electron may be approximated as follows:

$$E_{ABC} \approx E_A - E_B - E_C \tag{10.2}$$

Equation (10.2) demonstrates that the Auger electron energy is independent of the primary beam energy and is dependent only on the atomic energy levels. Therefore, the measured Auger electron energies are representative of the elemental composition of the sample surface. Because each element has a unique set of energy levels, each element has a unique set of Auger peaks. The KL_1L_3 Auger transition energy for Al, for example, may be calculated as follows:

$$\begin{aligned} E_{KL_1L_3} &\approx E_K - E_{L_1} - E_{L_3} \\ &\approx 1560 - 118 - 73 \\ &\approx 1369\,\text{eV}. \end{aligned}$$

The corresponding measured value is 1354 eV. We discuss two corrections that may account for this discrepancy.

Equation (10.2) must be modified by taking into account the spectrometer work function because Auger energies are typically referenced to the Fermi level. If the sample is in good electrical contact with the sample holder, the Fermi levels of the sample and instrument are identical. Hence, the kinetic energy of the ABC Auger electron may be approximated as follows:

$$E_{ABC} \approx E_A - E_B - E_C - \phi_A \,. \tag{10.3}$$

In the above expression, φ_A is the work function of the analyzer. Because the typical electron analyzer's work function is approximately 4 eV, equation (10.3) yields a value of 1365 eV for the KL_1L_3 Auger transition energy for Al. Now the discrepancy between the measured and calculated value has been reduced from 15 eV to 11 eV.

Equation (10.2), based on the binding energies of a neutral atom, can be further refined by taking into account the change in binding energy of a level that accompanies the formation of an ion.

$$E_{ABC} \approx E_A - E_B - E_C^* - \phi_A \,. \tag{10.4}$$

In the above expression, E_C^* is the binding energy of a level in the presence of a core hole. Equation (10.4) can be used to estimate Auger electron energies based on various empirical approximations [26]. More sophisticated semi-empirical methods have also been used to perform Auger electron kinetic energy calculations. The highest level of such Auger energy calculations involve relativistic *ab initio* computations, which take into account many body effects [27].

10.4 INSTRUMENTATION

Because an atomically clean surface needs to be maintained throughout the AES analysis process and because the electron beam needs to reach the sample without collisions with the intervening gas molecules, *turbo molecular pumps* (TMP) and/or ion pumps are usually employed to achieve ultrahigh vacuum conditions (10^{-9} torr and below) inside a stainless steel chamber equipped with metal seals. Vacuum locks in modern ultrahigh vacuum equipment allow for the introduction of new samples in less than 30 minutes without breaking the vacuum. Mu metal shielding inside the ultrahigh vacuum chamber may be necessary to minimize the effect of stray magnetic fields on the trajectory of electrons. In order to perform Auger analysis of grain boundaries, samples can be fractured *in situ* in ultrahigh vacuum [28]. Clean room compatible AES instrumentation for semiconductor analysis is now available from several manufacturers. Because the ability to finely focus electron beams allows for excellent spatial resolution, electron beams are the most popular choice in AES, although ionizing sources such as X-rays, ions, and positrons can also be used for Auger analysis.

The basic components of a typical Auger electron spectrometer (Figure 10.3) consist of the following: (1) electron source and electron optical column to form an electron probe onto the specimen surface; (2) an ion optical column for cleaning the sample surface and/or sputtering for depth profiling; (3) an electron energy analyzer; (4) a secondary electron detector and a pulse counter; (5) computer control and data display systems. The first four modules are located within the UHV chamber.

10.4.1 Electron Optical Column

In AES instrumentation, the electron beam from an electron source is focused onto the specimen surface by a suitable optical column. In addition to being monoenergetic, the electron beam used in AES instrumentation should be small in size with high brightness. The sample to be analyzed is irradiated with electrons with energy of 2–10 keV and beam current of 10^{-8} to 10^{-5} A. In the case of scanning Auger microscopy, energies as high as 35 keV and currents as low as 10^{-9} A are used to produce beam diameters as small as 100 Å. The electron source also should have a long life and high temporal stability. There are four main types of electron sources:

1. The tungsten thermionic emitter operates at a temperature of ~2700 K producing a low current density. Because of the low brightness and concurrent large beam size, the tungsten thermionic emitter is not optimal for Auger experiments that require good lateral resolution.
2. The lanthanum hexaboride (LaB_6) thermionic emitter, with a lower work function than tungsten, operates at a lower temperature (~1850 K)

and provides for good lateral resolution because it produces relatively high current density.

3. The cold field emitter, made of a tungsten single crystal, operates at room temperature in the presence of a high electrostatic field and produces high brightness. The cold field emitter is unstable in the presence of residual gases and hence requires pressures on the order of 10^{-10} torr.

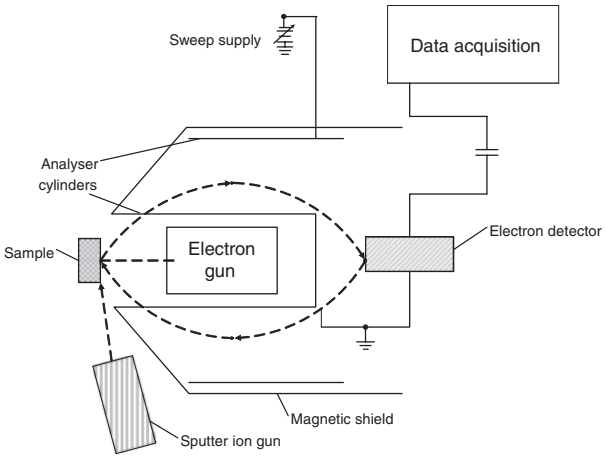

Figure 10.3 Top—A schematic representation of an Auger electron spectroscopy instrument. Bottom—A photograph of a commercial AES instrument (Physical Electronics).

4. The hot field emitter, also known as ZrO_2/W Schottky-type field emitter, operates at ~1800 K and produces high current densities.

Most modern AES instruments use either a LaB_6 or a Schottky type emitter as an electron source. The Schottky-type emitter is the preferred electron source for the highest resolution Auger instruments. A typical electron optical column with an electron source and other essential components is shown in Figure 10.4. It should be noted that some materials are susceptible to electron beam damage and therefore care must be exercised in examining such materials by AES.

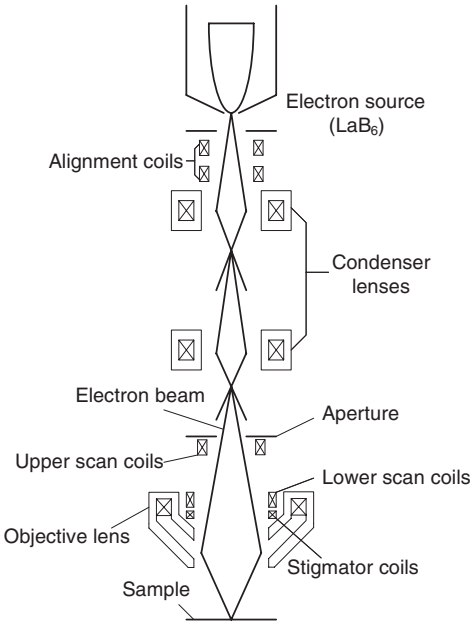

Figure 10.4 Schematic of electron gun used for Auger electron spectroscopy. Adapted from [10].

10.4.2 Ion Optical Column

For depth profiling and/or sputter cleaning, an electron impact-type ion source [16] is usually employed in conjunction with AES instruments. Electrons from a heated filament are accelerated by a cylindrical grid to an energy sufficient to ionize gas atoms by collisions. The resulting ions are accelerated into a focusing lens column. Inert gases such as argon (Ar) or xenon (Xe) are used in a typical electron impact-type ion source with a hot tungsten filament. Figure 10.5 shows a typical ion optical column with an electron impact ion source.

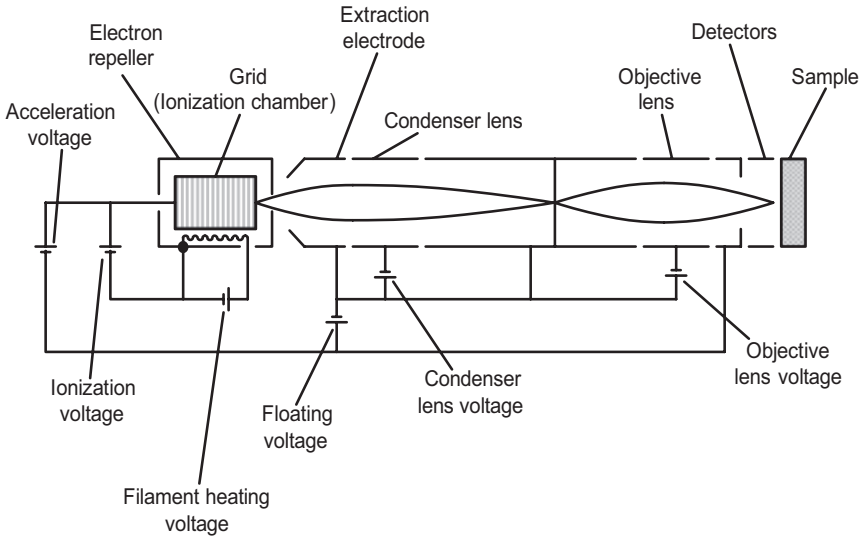

Figure 10.5 Schematic diagram of an ion optical column. Adapted from [10].

10.4.3 Electron Energy Analyzers

Electron energy analyzers are used to measure the number of ejected electrons (N) as a function of electron energy (E). The most commonly used energy analyzers in AES are: (i) the retarding field analyzer (RFA), (ii) the cylindrical mirror analyzer (CMA), and (iii) the concentric hemispherical analyzer (CHA).

Because of the limited energy resolution and poor signal-to-noise ratio resulting from mediocre transmission efficiency, the retarding field analyzer (Figure 10.6), commonly used for low energy electron diffraction studies, is not an optimal choice for Auger electron spectroscopy.

The high transmission efficiency, compact size, and ease of use of the cylindrical mirror analyzer (Figure 10.7) combine to make it the analyzer of choice for Auger electron spectroscopy.

Because of its higher resolution, the concentric hemispherical analyzer (Figure 10.8) is used in Auger electron spectroscopy when chemical state information is desired. The CHA consists of an input lens and the hemispherical analyzer. All XPS energy analyzers are concentric hemispherical analyzers.

The cylindrical mirror and concentric hemispherical analyzers are *band pass filters* in contrast to the retarding field analyzer (RFA), which is a *high pass filter*. The band pass filter allows passage of electrons within a band of energy (ΔE) at a pass energy (E), resulting in an energy resolution of $\Delta E/E$. Because the retarding field analyzer collects electrons with an energy greater than the specified energy E, the spectrum must be differentiated once to obtain the $N(E)$ spectrum.

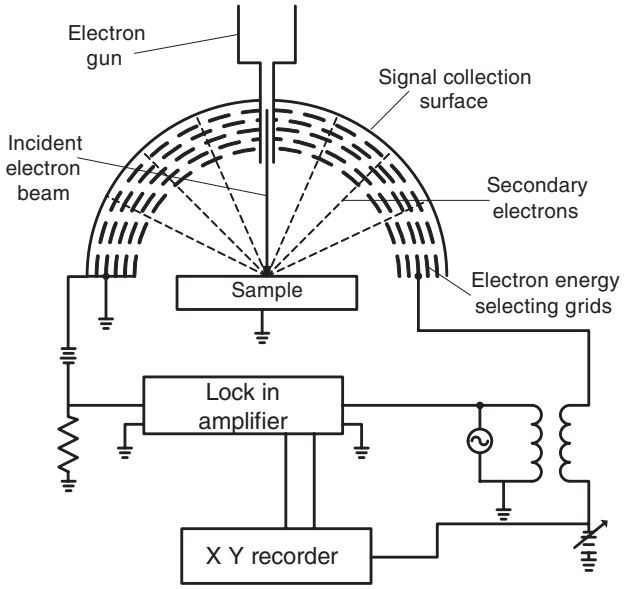

Figure 10.6 A schematic diagram of the retarding field analyzer. Adapted from [10].

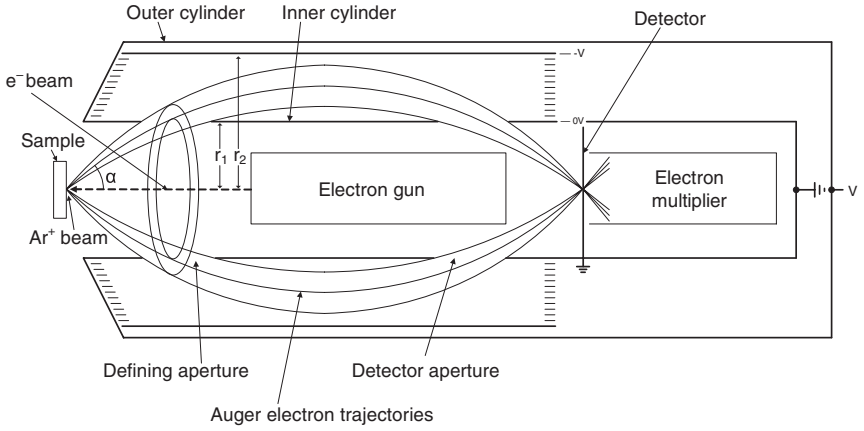

Figure 10.7 A schematic diagram of the cylindrical mirror analyzer. Adapted from various sources [10, 11].

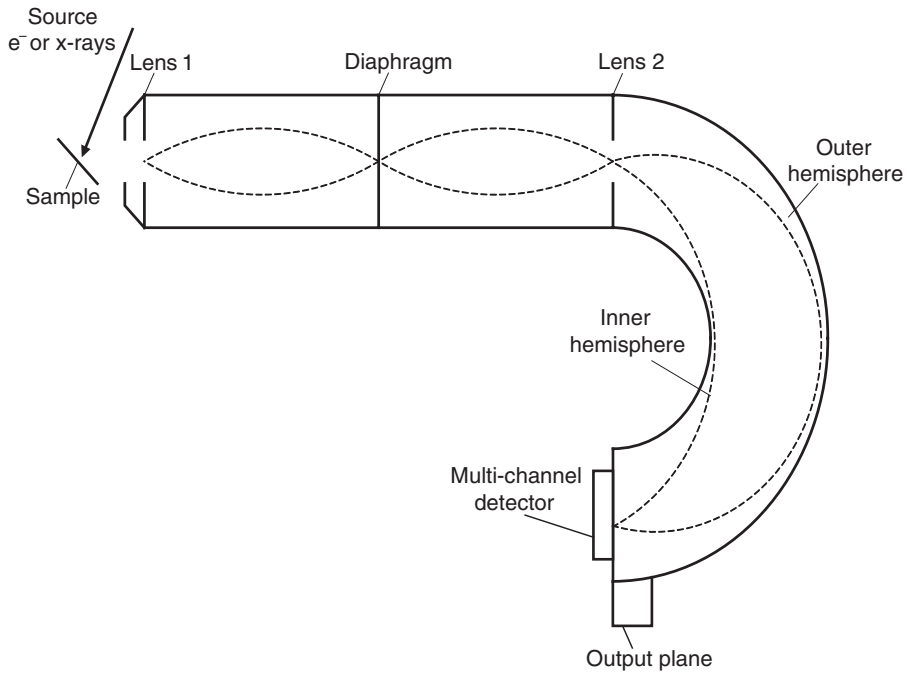

Figure 10.8 A schematic diagram of the concentric hemispherical analyzer. Adapted from [10].

10.4.4 Electron Detector

Electrons exiting the analyzer and arriving at the detector are amplified and counted by an electron multiplier, either a channeltron or a microchannel plate (MCP). Electrons striking the specially coated inside of a channeltron, a cone-shaped dynode, produce many secondary electrons, which are accelerated toward the anode. The many intervening collisions produce an avalanche effect, which results in a gain of ~10^8 for a channeltron. A microchannel plate consists of many tiny channeltrons fused together to form a disc. Electron intensity measurements are usually done by pulse counting.

10.4.5 Computer Control and Data Display Systems

Modern AES instrumentation has sophisticated computer control, data processing, and display systems. The computer control system has four major functions: (i) setting up conditions for analysis; (ii) acquiring and storing data efficiently; (iii) processing data; and (iv) displaying results in the form of spectra.

10.5 EXPERIMENTAL PROCEDURES INCLUDING SAMPLE PREPARATION

10.5.1 Sample

Both single crystal and polycrystalline solid samples can be analyzed with AES. Because a flat smooth sample enhances the quality of the Auger spectra, powders are pressed into the shape of a wafer before AES analysis. The specimen sample to be analyzed by Auger must be compatible with ultrahigh vacuum conditions. For example, a sample containing a significant amount of Zn is not suitable because of the high vapor pressure of Zn. Even if a suitable sample is placed in an ultrahigh vacuum chamber, additional treatment such as inert gas sputtering or ion etching to remove surface contaminants may be required before analysis. State-of-the-art AES instruments allow for samples as large as the 300 mm wafers used in the semiconductor industry.

While most metals and semiconductors are amenable to Auger analysis, insulators present a special problem. Charging of insulator samples during electron spectroscopy is problematic because: (1) kinetic energy measurements may be in error by as much as tens of eV, and (2) spectral peaks may be distorted due to inhomogeneous surface charge distribution [29]. Because an electron beam is used in Auger electron spectroscopy, charge compensation of insulator samples must be achieved by one or more methods: (1) lowering the incident electron beam energy to increase the emission of secondary electrons; (2) tilting the sample to decrease the angle between the sample surface and the beam and hence increase the number of electrons leaving the sample; (3) neutralizing the charge with low energy (~50 eV) positive ions such as Ar^+; (4) placing thin films of the insulating sample on a conductive surface such as graphite; and (5) decreasing the incident current density [29, 30]. Such techniques allow the analysis of insulators such as ceramics [31].

10.5.2 Beam Effects and Surface Damage

Electron beam damage to specimens is a concern with Auger electron spectroscopy. Examples of electron beam-induced surface damage include: (1) creation of defects, (2) change of crystal structure, (3) change of surface topography, (4) change of oxidation state, (5) bond cleavage, (6) adsorption, (7) desorption, and (8) segregation [32].

In order to minimize damage, checks for the presence of specimen damage must be performed routinely during analysis. If damage is detected, the experimental conditions can be adjusted to minimize surface damage. Electron beam effects may be reduced by: (1) decreasing the electron beam energy, (2) decreasing the current density at the surface by defocusing the

beam, and/or (3) reducing the time of exposure by rastering the beam over a selected area. Reducing sample temperature during electron irradiation was found to minimize radiation damage to polymers during Auger analysis [33].

10.5.3 AES Modifications and Combinations with Other Techniques

The basic technique of AES as described earlier has also been adapted for use in Auger depth profiling, which provides quantitative compositional information as a function of depth below the surface, and scanning Auger microscopy, which provides spatially resolved information on the composition of surfaces. Auger depth profiling and scanning Auger microscopy will be discussed later in this chapter.

Auger electron spectroscopy can be combined with other analytical techniques for simultaneous analysis. For example, AES is combined with energy dispersive X-ray spectroscopy (EDS or EDX) for elemental analysis and secondary ion mass spectroscopy (SIMS) for trace impurity analysis [10]. Auger instruments can also be equipped with an X-ray source for X-ray photoelectron spectroscopy (XPS). Similarly, XPS instruments can also be equipped with an electron gun for simultaneous AES analysis.

10.6 AUGER SPECTRA: DIRECT AND DERIVATIVE FORMS

Auger spectra are usually acquired and displayed in one of two ways: (a) *direct form,* where the total electron signal is measured as a function of the kinetic energy of the electrons leaving the sample; (b) *derivative form,* where the derivative of the total electron signal is measured as a function of kinetic energy. The derivative spectrum helps to accentuate the Auger signal by suppressing the background due to secondary and backscattered electrons, as described below.

The interaction of an electron beam with a solid sample results in the emission of secondary and backscattered electrons whose distribution plotted as a function of kinetic energy is shown in Figure 10.9.

The schematic secondary and backscattered electron distribution shown in this figure demonstrates four features (right to left):

(1) The strong peak at the incident electron energy is due to elastically back- scattered primary electrons.
(2) The loss peaks at discrete energies on the low energy side of the elastic peak are due to electrons that have lost energy to surface and bulk plasmons.
(3) The sharp peaks that are independent of primary beam energy are due to Auger electrons.

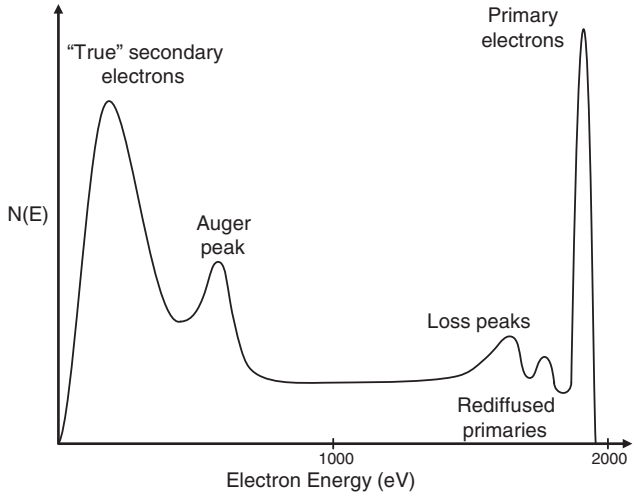

Figure 10.9 Schematic diagram of the energy distribution of secondary and backscattered electrons produced by the interaction of a nearly monochromatic electron beam with a solid. Adapted from [9].

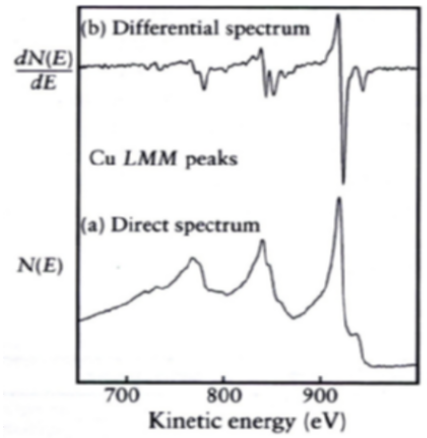

Figure 10.10 The direct and differentiated spectrum of copper [11]. (Copyright John Wiley & Sons, Ltd. Reproduced with permission.)

(4) The broad peak at low energies (< 50 eV) is due to secondary electrons that have undergone multiple inelastic collisions within the solid.

Because the low intensity Auger peaks are superimposed on a large slowly varying background signal, the $N(E)$ vs. E spectrum is differentiated to yield the differentiated spectrum, $dN(E)/dE$ vs. E, in which the Auger peaks are accentuated with respect to the background signal, as exemplified in Figure 10.10. The main peaks, which are characteristic of Cu, appear between 700 and 1000 eV. The background, due to the secondary electrons gene-

rated by inelastic scattering of electrons, is fairly extensive in the direct spectrum. The AES spectrum for Cu demonstrates that because the background is considerably reduced in the differentiated form the sensitivity of detection is enhanced. Direct spectra, however, are now being used more frequently because of easier quantification. The absence of secondary electrons in the gas phase makes direct spectra the ideal choice.

10.7 APPLICATIONS

10.7.1 Qualitative Analysis

Elemental analysis of surfaces is based on the kinetic energies of the observed Auger transitions. For positive identification it is necessary to match not only energies but also the shapes and relative strengths of the observed Auger peaks [34]. Modern AES instrumentation makes use of computer programs for rapid Auger peak identifications. However, such identification must be done with care, especially when two or more elements have overlapping or nearly overlapping Auger peaks. Given the new international standards [25], incorrect calibration of the kinetic energy scale should in the future not contribute to additional uncertainty in element identification. As in most other spectroscopic methods, conclusive identification of elements is facilitated if the reference and sample Auger spectra are both obtained on the same instrument [34].

The first step in qualitative Auger analysis involves obtaining a survey spectrum with relatively modest resolution in a fairly short time. Survey Auger spectra are typically recorded at energies between 0 eV and 1000 eV because most elements have significant Auger transitions in this range. Moreover, Auger electrons with energies greater than 1000 eV are less surface-sensitive because these electrons have longer inelastic mean free paths. Because Auger features are much more pronounced in derivative spectra, such spectra are commonly used in qualitative AES investigations.

Each element has a set of characteristic Auger peaks, as demonstrated by a plot of the Auger electron energy as a function of atomic number (Z) (Figure 10.11). The figure demonstrates that the Auger transitions of choice for the different elements can be summarized as follows: $3 < Z < 14$ (KLL transitions), $14 < Z < 40$ (LMM transitions), $40 < Z < 82$ (MNN transitions), and $82 < Z$ (NOO transitions).

10.7.2 Quantitative Analysis

The goal of quantitative analysis by AES is to determine the chemical composition of solid surfaces by calculating atomic concentrations from Auger peak intensity measurements. In the case of a direct Auger spectrum,

peak intensities are obtained from peak area measurements following a suitable baseline subtraction. In the case of a derivative spectrum, peak intensities are characterized by the peak-to-peak heights. The direct spectrum is preferred for most AES quantification studies. Estimating the in-depth distribution of elements is important in the AES quantification of surface elemental concentration. Even if the solid composition is uniform down to a depth of a few nanometers, the surface concentration may not be proportional to the measured peak intensity. More accurate quantification can be achieved if the peak shape is also taken into consideration when performing Auger surface analysis.

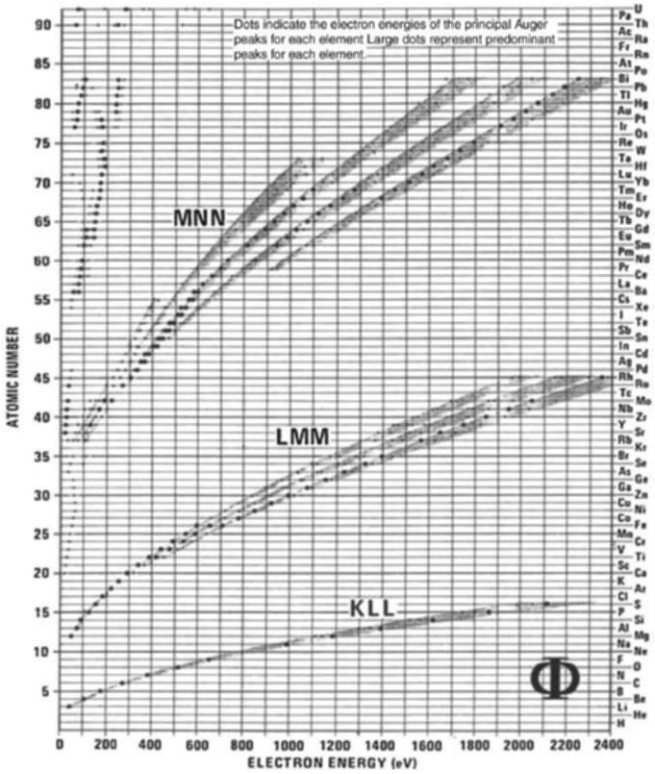

Figure 10.11 Principal Auger electron energies for each element. The larger dots correspond to prominent Auger peaks [35]. (Copyright Physical Electronics, Eden Praire, MN. Reproduced with permission.)

Reproducibility of Auger intensity ratios may be compromised by: (1) problems with sample alignment, (2) deflections of electrons by stray magnetic fields, and (3) energy-dependent detector efficiencies [36]. A comprehensive review of Auger and XPS quantification methods was published in 1996 [37].

We describe in detail below the three methods used for Auger quantification: (1) first principles Auger intensity calculations, (2) standards of known composition, and (3) elemental relative sensitivity factors.

10.7.2.1 First Principles Auger Intensity

The measured Auger current intensity (I_A) can be related to the depth (z) dependent atomic density $N_A(z)$ by considering the physical principles underlying (1) Auger electron generation, (2) transport of the Auger electron through the solid matrix, and (3) detection of the Auger electron. The resulting relationship is as follows:

$$I_A = I_o G \sigma_A G_{CK} \gamma_A K (1 + r_M) \int_{z=0}^{\infty} N_A(z) \exp\left[\frac{-z}{\lambda_A \cos\theta}\right] dz \; fTD. \tag{10.5}$$

In the above are the following variables: I_A is the measured Auger current from element A, I_o is the incident electron current (primary beam current), G is a geometrical factor accounting for the area under irradiation (depends on angle of incidence of primary beam), σ_A is the ionization cross-section (a function of incident electron energy and the atomic level being ionized), G_{CK} is the Coster-Kronig yield correction, γ_A is the Auger yield factor (corrects for X-ray fluorescence), K is the sample condition factor (surface roughness, contamination, etc.), r_M is the matrix-dependent backscattering factor that accounts for additional ionizations due to backscattered primary electrons, z is the depth below the surface, N_A is the number density of atoms of type A, λ_A is the matrix- and Auger electron energy-dependent inelastic mean free path (related to attenuation length and the effective escape depth), θ is the Auger electron's take-off angle, measured from the surface normal, f is the analyzer retardation factor (for RFA analyzer; not needed for CMA), T is the analyzer transmission factor (a function of energy), and D is the detector efficiency factor (a function of energy and time).

Most of the above terms are constants for a given set of experimental conditions and for a particular Auger transition. Moreover, the integral can be simplified by assuming that the concentration is uniform over a depth of ~5λ_A, as shown below:

$$\begin{aligned} I_A &= I_o G \sigma_A G_{CK} \gamma_A K (1 + r_M) N_A fTD \int_{z=0}^{\infty} \exp\left[\frac{-z}{\lambda_A \cos\theta}\right] dz \\ &= I_o G \sigma_A G_{CK} \gamma_A K (1 + r_M) N_A fTD \lambda_A \cos\theta. \end{aligned} \tag{10.6}$$

Although absolute Auger quantification using the above equation is not practical for most cases, this equation provides a theoretical basis for understanding other quantification methods described below.

10.7.2.2 Standards of Known Composition

Relative Auger quantification is performed by keeping many of the experimental parameters in equation (10.6) fixed and by using locally produced standards of known composition. Instrumental variables are

eliminated in this ratio technique because the same instrument is used to analyze both the *test* and *standard* samples. The ratio of the measured Auger current from the test ($I_{\mathrm{A}}^{\mathrm{T}}$) and standard samples ($I_{\mathrm{A}}^{\mathrm{S}}$) is given by

$$\frac{I_{\mathrm{A}}^{\mathrm{T}}}{I_{\mathrm{A}}^{\mathrm{S}}} = \frac{(1+\mathrm{r}_{\mathrm{M,A}})_{\mathrm{T}}}{(1+\mathrm{r}_{\mathrm{M,A}})_{\mathrm{S}}} \frac{\lambda_{\mathrm{A}}^{\mathrm{T}}}{\lambda_{\mathrm{A}}^{\mathrm{S}}} \frac{N_{\mathrm{A}}^{\mathrm{T}}}{N_{\mathrm{A}}^{\mathrm{S}}}. \tag{10.7}$$

In the above expression, N_A^T and N_A^S are the number densities of A in the test and the standard samples. Equation (10.7) may be rewritten as follows:

$$\frac{N_{\mathrm{A}}^{\mathrm{T}}}{N_{\mathrm{A}}^{\mathrm{S}}} = \frac{(1+\mathrm{r}_{\mathrm{M,A}})_{\mathrm{S}}}{(1+\mathrm{r}_{\mathrm{M,A}})_{\mathrm{T}}} \frac{\lambda_{\mathrm{A}}^{\mathrm{S}}}{\lambda_{\mathrm{A}}^{\mathrm{T}}} \frac{I_{\mathrm{A}}^{\mathrm{T}}}{I_{\mathrm{A}}^{\mathrm{S}}}. \tag{10.8}$$

If the composition of the test sample is close to that of the standard, the influence of the matrix on electron backscattering and inelastic mean free path may be ignored and the above equation may be used to obtain the number density of the test sample directly from the ratio of the Auger yields:

$$\frac{N_{\mathrm{A}}^{\mathrm{T}}}{N_{\mathrm{A}}^{\mathrm{S}}} = \frac{I_{\mathrm{A}}^{\mathrm{T}}}{I_{\mathrm{A}}^{\mathrm{S}}}. \tag{10.9}$$

More generally, it is necessary to evaluate the ratios of the backscattering factors and the inelastic mean free paths to determine the composition of the test sample. Because evaluating these matrix effects can be rather complicated, a new method to quantify AES and XPS data has been proposed based on angle-averaged reflected electron energy loss spectroscopy (REELS) spectra and involving "average matrix sensitive factors" [40].

10.7.2.3 Elemental Sensitivity Factors

This quantitative Auger method is based on the assumption that matrix effects can be ignored. With this assumption, equation (10.6) can be simplified as follows:

$$I_{\mathrm{A}} = s_{\mathrm{A}} N_{\mathrm{A}}. \tag{10.10}$$

In the above expression, s_{A} is the Auger sensitivity factor of element A. Relative Auger sensitive factors are defined relative to A and tabulated. If the sample contains two elements A and B, the number density N_{A} of A is given by the following expression:

$$N_{\mathrm{A}} = \frac{\left(\frac{I_{\mathrm{A}}}{s_{\mathrm{A}}}\right)}{\left(\frac{I_{\mathrm{A}}}{s_{\mathrm{A}}} + \frac{I_{\mathrm{B}}}{s_{\mathrm{B}}}\right)}. \tag{10.11}$$

10.7.3 Chemical Information

While elements present on the surface can be positively identified by the Auger peak energies, changes in chemical state (e.g., oxidation state) or chemical environment can be deduced from changes in Auger peak positions, intensities, and shapes. As such, AES spectra, particularly derivative spectra, are used as "chemical fingerprints" for identification and characterization. The classic example of such *qualitative* analysis involves the carbon KLL Auger spectra for molybdenum carbide, silicon carbide, graphite, and diamond (Figure 10.12) [39]. The spectra show variations in lineshapes due to differences in the chemical environments of the carbon atoms in the four samples. Although the data clearly show that bonding information can be obtained from Auger spectroscopy, obtaining chemical state and chemical environment information from Auger spectra is challenging because the Auger process involves three energy levels. More detailed electronic structure information (e.g., hybridization, electron delocalization, screening effects) may be obtained from *quantitative* spectral lineshape analysis, a daunting task that is currently beyond the scope of most Auger practitioners [40].

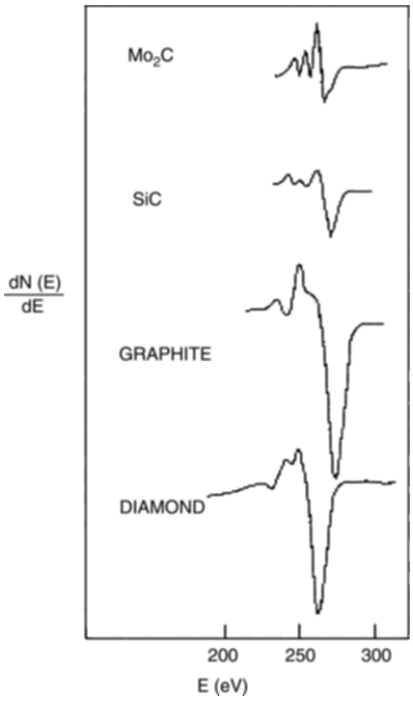

Figure 10.12 Effect of chemical environment on the KLL Auger spectra of carbon [39]. The shift in the Auger peak energy for diamond is due to charging of the insulator. (Reproduced with permission from the American Institute of Physics.)

Chemical shifts, or, equivalently, energy shifts, occur when there is a charge transfer from one atom to another. For example, atomic oxygen adsorbed on clean metal surfaces can produce measurable shifts in energies of Auger peaks from metals. Auger spectra of aluminum in AlN, AlF_3, AlB_2 and Al_2O_3 (Figure 10.13) clearly show the phenomena of chemical shifts in Auger spectroscopy.

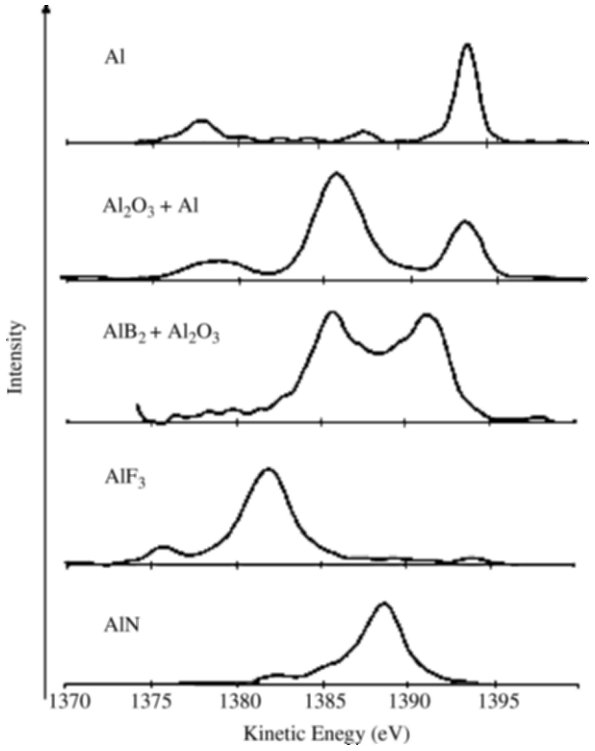

Figure 10.13 Chemical shifts demonstrated in the Auger KLL spectra of several Al compounds [41]. (Copyright John Wiley & Sons Ltd. Reproduced with permission.)

Several metal LVV and MVV lineshapes have also been used extensively for Auger chemical fingerprinting to study the effects of hydrogen or oxygen exposure, intercalation, or changes in crystal structure. Auger chemical fingerprinting has also been used to analyze the $L_3M_{23}V$ Auger lineshape of high-temperature superconductors [42].

10.7.4 Auger Depth Profiling

Obtaining the chemical composition as a function of depth below the surface using Auger electron spectroscopy is referred to as "Auger depth profiling,"

one of four modes of Auger operation (point analysis, line scan, and surface imaging the other three modes of Auger operation). Industrial applications of Auger depth profiling include analyzing microelectronics devices, investigating corrosion-resistant surfaces, and characterizing plasma-modified surfaces [43]. Auger depth profiling methods may be broadly categorized as follows: (1) nondestructive, (2) sputtering by noble gas ions, and (3) mechanical sectioning. Brief summaries of methods 1 and 2 are given below. Interestingly, Auger sputter depth profiling (method 2) has become the most popular choice for chemical analysis of thin films [44].

10.7.4.1 Nondestructive Methods

Angle-resolved Auger electron spectroscopy (ARAES) allows for non-destructive depth profiling but works for only very thin layers up to a thickness of approximately 100 Å. Auger depth profiling may be accomplished by changing the geometry of the experiment because the depth of analysis depends on the emission angle of the Auger electron. While angle-resolved X-ray photoelectron spectroscopy has been extensively used for non-destructive depth profiling, the use of angle-resolved Auger for such analysis has been somewhat limited [45, 46].

10.7.4.2 Sputter Depth Profiling

Auger sputter depth profiling usually involves simultaneous Auger elemental analysis and inert gas (argon or xenon) ion bombardment sputtering (etching) with an ion gun to remove material from the surface in a controlled manner to expose underlying atomic layers. Although Auger *survey* scans can be performed during sputter depth profiling, Auger analysis within pre-selected energy windows allows for more rapid data acquisition. Depth profiling with Auger may also be performed sequentially with alternating cycles of sputtering and analysis by AES. An example of Auger sputter depth profiling is shown in Figure 10.14.

Despite the popularity of sputter profiling with Auger, many studies have documented the complexities inherent in this technique [47]. Auger sputter depth profiling is challenging due to ion beam-induced changes in surface roughness and composition, changes that are associated with effects such as preferential sputtering (one element is sputtered faster than another element in the matrix) [48], collisional mixing, and ion-induced reactions (e.g., metal surface oxide is reduced to metal [8]). Such complexities associated with AES sputter depth profiling experiments make difficult the task of converting Auger intensities measured as a function of sputtering time into elemental concentration as a function of depth. Despite formidable challenges, recent developments in the modeling of sputtering, such as the so-called *mixing roughness information* (MRI) depth model, allow for depth analysis of nanostructures [49].

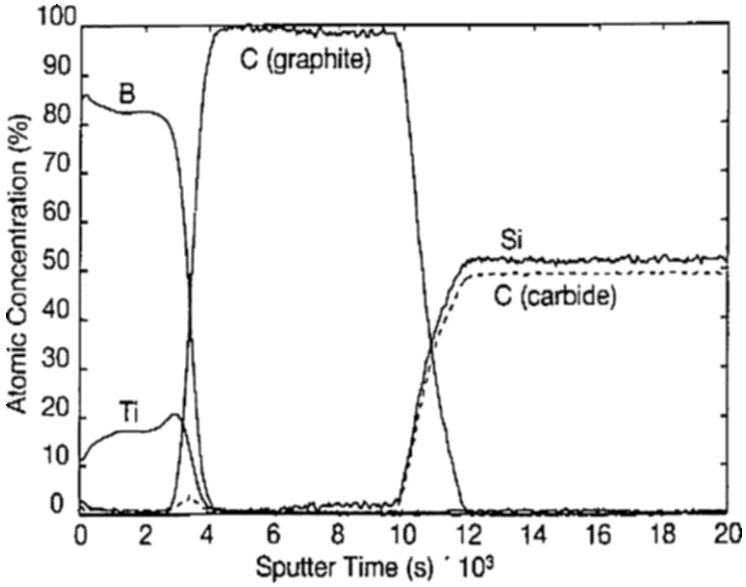

Figure 10.14 Auger sputter depth profile of a TiB_2/C-coated SiC filament [9]. (Reproduced by permission of Taylor & Francis Group, LLC, http:/www.taylorandfrancis.com)

In addition to advances in theory, several experimental innovations have made sputter depth profiling with Auger more precise. For example, collisional atomic mixing, which degrades depth resolution, may be minimized by using ultralow ion energies (< 500 eV) instead of the typical high ion energies (several keV). The low ion energies, however, result in low beam current densities, which yield etching rates below 0.2 nm min^{-1} [50]. A more acceptable etching rate of 1 nm min^{-1} and a high depth resolution of 2 nm has been achieved with a specially designed ion gun capable of producing ion currents of $\sim 10^{-6}$ A at ion energies as low as 100 eV [50]. The use of such ultralow ion energies, however, is complicated by enhanced preferential sputtering, as demonstrated recently for the GaAs/AlAs superlattice, an ISO reference material [51].

A second example of experimental innovation involves sample rotation during Auger sputter depth profiling [52]. Because this so-called Zalar rotation technique time-averages the angles between the ion beam and the various crystalline planes, sample roughening is minimized and, consequently, depth resolution is enhanced. This feature in now available in commercial Auger instruments such as the PHI 700 manufactured by Physical Electronics.

Auger sputter depth profiling requires stringent ultrahigh vacuum conditions because the surface exposed by sputtering may act as a getter for residual gases. Moreover, for the same reason, the noble gas used for sputtering must be of the highest purity [11].

10.7.5 Auger Images and Linescans

Scanning Auger microscopy involves the acquisition of Auger data as a function of two-dimensional position within a defined area on a specimen. With an excellent lateral resolution of less than 10 nm, scanning Auger microscopy can be used effectively to image nanoscale structures and to produce two-dimensional maps of surface elemental composition. In combination with XPS, scanning Auger microscopy has been used recently to successfully analyze archeological artifacts such as ancient metal surfaces [53]. The large amount of data collected during each scan poses a significant challenge for data storage [54]. Adequate image quality also requires times on the order of hours to acquire Auger maps [54]. Progress in scanning Auger microscopy has been recently reviewed [55].

Sophisticated scanning Auger microscopy instrumentation is commercially available from several vendors, including Physical Electronics, JEOL, SPECS and STAIB Instruments. In addition to the standard components found in a typical Auger spectrometer, a scanning Auger microscope contains a secondary electron detector (SED) for performing secondary electron microscopy (SEM) imaging (Figure 10.15). Such imaging provides surface topographic information that may be correlated to information obtained from Auger electron spectroscopy. Moreover, by taking account of the background signal, secondary electron microscopy may be used to suppress topographic information and enhance chemical information when performing scanning Auger microscopy, as demonstrated in Figure 10.16.

While an Auger map shows the relative elemental concentration as a function of x and y, an Auger linescan measures the relative elemental concentration as a function of x along a straight line on a sample. As with scanning Auger microscopy, a scanning electron image provides the means to choose the analysis line.

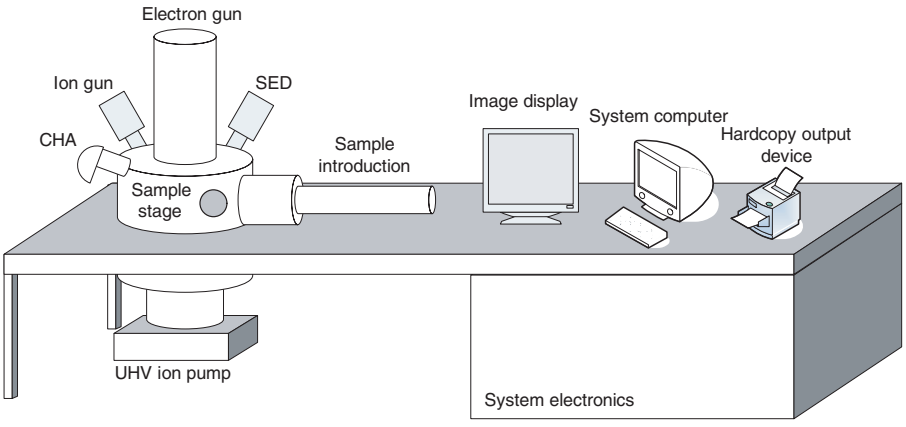

Figure 10.15 Schematic diagram of a scanning Auger microscope. Adapted from [9].

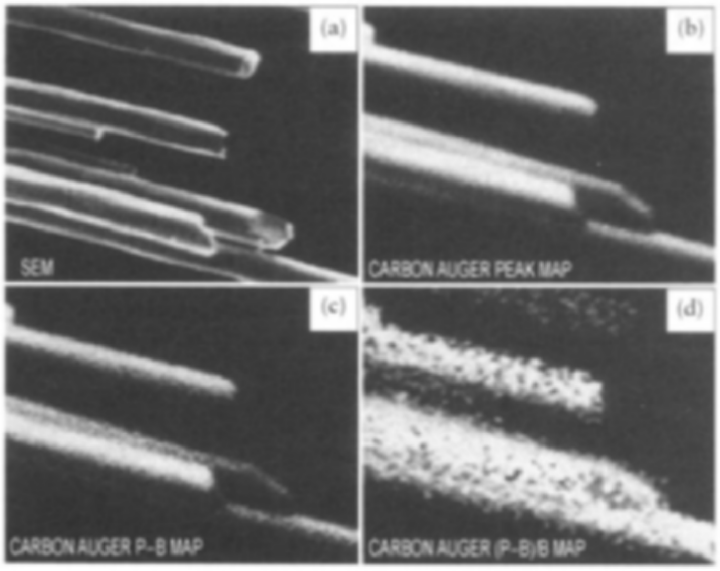

Figure 10.16 Scanning Auger microscopy of carbon fibers: (a) SEM image, (b) peak map of carbon Auger electrons, (c) peak background map, and (d) correction for topographic effects [11]. (Copyright John Wiley & Sons Ltd. Reproduced with permission.)

10.7.6 Research and Industry

In addition to being used as a tool in surface science research, both basic and applied, Auger electron spectroscopy is widely used in industry as an analytical tool to investigate surfaces, interfaces, thin films, and submicron features. In the thin film industry, AES depth profiling is routinely carried out for monitoring chemical composition. Auger is especially useful for detecting small defects (< 500 Å) that may play a critical role in the fabrication of small semiconductor devices. Recent experiments have demonstrated the utility of AES for investigating biomaterials such as hydroxyapatite [56]. The other areas of Auger applications are found in catalysis, solid state reactions, metallurgy, corrosion, advanced ceramics, and structural materials. A few of these applications are discussed in more detail below.

10.7.6.1 Corrosion

While XPS is ideally suited to characterize the growth of passivating thin films that inhibit the corrosion of stainless steel, submicron scanning Auger spectroscopy, with its high spatial resolution, is very useful for studying microscopic inclusions (chemical inhomogeneities) present in these protective thin films [11]. These inclusions, acting as pit initiation sites, are known to

compromise the corrosion resistance of stainless steel in the presence of chloride ions [57].

10.7.6.2 Ceramics

Despite problems with charging of insulator samples, Auger electron spectroscopy has been used to study ceramic thin film materials. For example, Auger depth profiling was recently employed to characterize sol-gel-derived $Pb(Mg_{1/3}Nb_{2/3})_{0.7}Ti_{0.3}O_3$ (PMNT) thin films, a type of ferroelectric oxide thin film that has potential applications in electro-optic, pyroelectric, and micro electromechanical devices [58]. The Auger depth profile (intensity as a function of sputter time) shown in Figure 10.17 demonstrates the uniform deposition of a PMNT thin film on a platinum electrode.

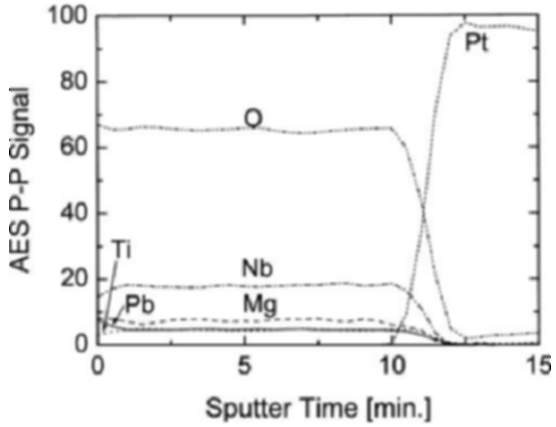

Figure 10.17 An Auger depth profile of a lead magnesium niobium titanate (PMNT) thin film [58]. (Reproduced with permission from the Institute of Applied Physics, Japan.)

10.7.6.3 Semiconductor Industry

The surface sensitivity of Auger electron spectroscopy has been extensively exploited in many laboratories for semiconductor research. In addition to surface sensitivity, Auger electron spectroscopy is also very useful for performing high resolution depth analysis of the layered material in semiconductor devices. The relatively flat interfaces present in such devices are especially amenable to analysis by Auger electron spectroscopy sputter depth profiling [11]. Such Auger depth profile studies have yielded information important for understanding interface purity, thickness, and diffusion [11]. Moreover, Auger electron spectroscopy can be used to combine depth and chemical state information in semiconductor devices

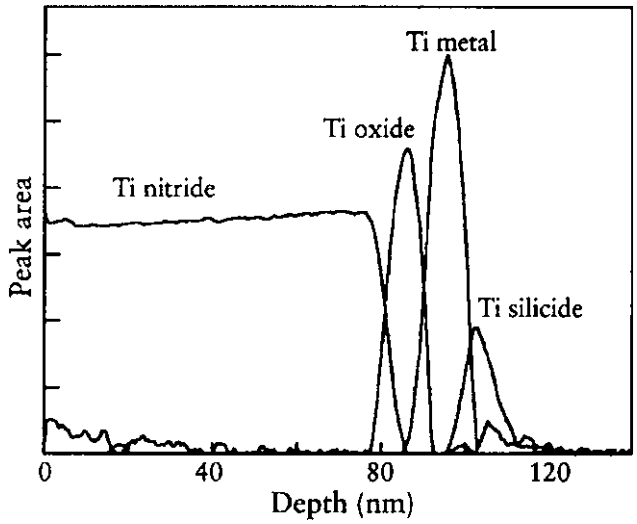

Figure 10.18 Depth profile of a semiconductor material consisting of silicon and various compounds of titanium [11]. (Copyright John Wiley & Sons Ltd. Reproduced with permission.)

(Figure 10.18). It is interesting to note that AES has also been used to characterize room temperature single electron transistors (SET), which represent a potential breakthrough in the quest for even smaller devices [59].

Because of shrinking device dimensions, AES has recently become a vital tool in the semiconductor industry for process control and failure analysis [60]. For example, because of its excellent spatial resolution and non-destructive nature, AES is ideally suited to identify and characterize submicron semiconductor defects (as small as 500 Å) which are beyond the capabilities of conventional methods based on X-ray dispersive analysis tools [61]. An Auger defect review tool (DRT) capable of analyzing 200-mm thick wafers has been developed and evaluated [62–64]. Despite the demanding requirements for ultrahigh vacuum, a recent publication has recommended that AES and XPS analysis be moved from laboratory settings to the production line in integrated circuit manufacture [65].

10.8 RECENT ADVANCES

Recent developments in the theory of Auger spectroscopy, especially those dealing with electron correlation, have been comprehensively reviewed [66]. We briefly review two of the Auger experimental techniques that have undergone rapid growth in the last decade or two.

10.8.1 Positron-Annihilation-Induced AES

First demonstrated in 1988 [67], positron-annihilation-induced Auger electron spectroscopy (PAES) involves the detection of electron emission due to Auger transitions initiated by positrons (the antiparticles of electrons) annihilating core electrons. The basic principles of AES and PAES are compared in Figure 10.19.

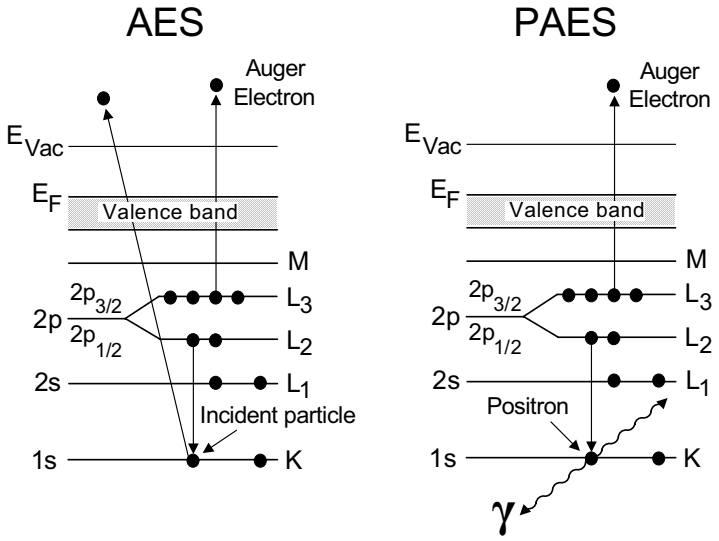

Figure 10.19 Comparison of basic principles of AES and PAES.

Compared to the traditional high energy electron-induced AES, PAES offers several advantages: (1) surface sensitivity is enhanced because positrons are trapped in an image potential on the surface prior to annihilation; (2) beam-induced damage is minimized because very low energy (~15 eV) positrons are used; and (3) background of secondary electrons is drastically reduced because the energy of the positrons is too low to excite secondary electrons. Recent applications of PAES include distinguishing the different crystallographic planes in semiconductors [68], determining Auger lineshapes [69], detecting surface impurities [70], and studying the growth dynamics of thin films [71].

10.8.2 Auger Photoelectron Coincidence Spectroscopy

Auger photo electron coincidence spectroscopy (APECS) is a powerful new experimental technique to characterize a number of important properties such as local electronic structure in novel solids including high temperature superconductors [72]. In addition, despite the many challenges associated with these measurements, APECS is considered a valuable tool for

simplifying complex Auger spectra, thereby enabling a fundamental understanding of the physical processes, including electron-electron correlation, governing such spectra [73]. In a typical APECS experiment the sample is irradiated with X-rays that excite both a core photoelectron and an Auger electron, both of which are detected in coincidence (at the same time) using two electron energy analyzers. By allowing the separation of overlapping Auger peaks, APECS is particularly useful for analyzing samples containing more than one element [74]. Very recent results of APECS experiments have demonstrated the technique's extreme surface sensitivity [75] and ability to discern the emission depth of Auger electrons [76].

10.9 CONCLUSIONS

Auger electron spectroscopy has been used to study the surface and interfacial properties of semiconductor devices, catalysts, metals, advanced ceramics, biomaterials, and other novel materials. Advances during the past four decades in Auger instrumentation have made possible the transition from research and development to more practical applications such as quality control and failure analysis [21]. Auger electron spectroscopy will continue to make pivotal contributions to the continuing revolution in material science.

ACKNOWLEDGMENTS

The authors thank Wesley R. Nieveen and Ronald E. Negri for their assistance in review of the manuscript and Lin Zhu for assistance with preparation of figures. R.P.G was supported by a grant from the National Science Foundation (NSF grant number CHE–0455278).

REFERENCES

[1] Allenspach, R., Mauri, D., Taborelli, M. & Landolt, M. (1987) *Phys. Rev. B* **35** (10), 4801.
[2] Bruhwiler, P.A., Karis, O. & Martensson, N. (2002) *Reviews of Modern Physics* **74** (3), 703.
[3] Yue, F., Swineford, R.S. & Pappas, D.P. (1996) *Phys. Rev. B* **53** (12), 8036.
[4] Ramaker, D.E., Fry, R.A. & Idzerda, Y.U. (1995) *J. Electron Spectrosc. Relat. Phenom.* **72**, 169.
[5] Auger, P. (1925) *J. Phys. Radium* **6**, 205.
[6] Meitner, L. (1923) *Z. Phys.* **17**, 54.
[7] Diehl, S., Cubaynes, D., Kennedy, E.T., Wuilleumier, F.J., Bizau, J.M., Journel, L., VoKy, L., Faucher, P., Hibbert, A., Blancard, C., Berrah, N., Morgan, T.J., Bozek, J. & Schlachter, A.S. (1997) *J. Phys. B-At. Mol. Opt. Phys.* **30** (18), L595.
[8] Dastoor, P.C. (2003) *Springer Series in Surface Sciences* **23**, Surface Analysis Methods in Materials Science (2nd Ed.), 155.

[9] Narumand, D.H. & Childs, K.D. (1999) *Applied Spectroscopy Reviews* **34** (3), 139.
[10] Briggs, D. & Grant, J.T. (Eds.) (2003) *Surface Analysis by Auger and X-Ray Photoelectron Spectroscopy* IMPublications and SurfaceSpectra, Chichester, UK and Manchester, UK.
[11] Watts, J.F. & Wolstenholme, J. (2003) *An Introduction to Surface Analysis by XPS and AES*. John Wiley & Sons Ltd., Chichester.
[12] Gergely, G. (1994) *Vacuum* **45** (2-3), 311.
[13] Lander, J.J. (1953) *Phys. Rev*. **91** (6), 1382.
[14] Harris, L.A. (1968) *Appl. Phys*. **39** (3), 1419.
[15] Taylor, N.J. (1969) *Rev. Sci. Instrum.* **40** (6), 792.
[16] Palmberg, P.W. & Bohn, G.K. (1969) Tracy, J.C. *Appl. Phys. Lett.* **15** (8), 254.
[17] Macdonal. Nc, Waldrop, J.R. (1971) *Appl. Phys. Lett.* **19** (9), 315.
[18] Barkshire, I.R., Roberts, R.H. & Prutton, M. (1997) *Appl. Surf. Sci.* **120** (1-2), 129.
[19] Prutton, M., Barkshire, I. R. & Crone, M. (1995) *Ultramicroscopy* **59** (1-4), 47.
[20] Palmberg, P. W. (1972) Vac. J. *Sci. Technol.* **9** (1), 160.
[21] Powell, C. J. (2003) Vac. J. *Sci. Technol. A* **21** (5), S42.
[22] Seah, M. P. (2003) *Surface Analysis by Auger and X-Ray Photoelectron Spectroscopy*, 167.
[23] Seah, M.P. (2004) *Surf. Interface Anal.* **36** (13), 1645.
[24] Seah, M.P. (2003) *Surf. Interface Anal.* **35** (3), 327.
[25] Seah, M.P. (2003) *Surf. Interface Anal.* **35** (3), 329.
[26] Chung M.F. & Jenkins, L.H. (1970) *Surf. Sci.* **22** (2), 479.
[27] Ishii, T., Kover, L., Berenyi, Z., Cserny, I., Ikeno, H., Adachi, H. & Drube, W. (2004) *J. Electron Spectrosc. Relat. Phenom.* **137-40**, 451.
[28] Smith J.F. & Southworth, H.N. (1981) *Journal of Physics E- Scientific Instruments* **14** (7), 815.
[29] Kelly, M.A. (2003) in *Surface analysis by Auger and X-Ray Photoelectron Spectroscopy*, edited by D. Briggs and J. T. Grant IMPublications and SurfaceSpectra, Chichester, UK and Manchester, UK.
[30] Hofmann, S. (1992) *J. Electron Spectrosc. Relat. Phenom.* **59** (1), 15.
[31] Watts, J.F. (1993) *British Ceramic Proceedings* **51**, (Nanoceramics), 195.
[32] Baer, D.R., Engelhard, M.H., Gaspar, D.J. & Lea, A.S. (2003) in *Surface Analysis by Auger and X-Ray Photoelectron Spectroscopy*, edited by D. Briggs and J.T. Grant (IMPublications and SurfaceSpectra, Chichester, UK and Manchester, UK,).
[33] Sekine, T., Ikeo, N., Nagasawa, Y. & Kikuma, J. (1995) *Surf. Interface Anal.* **23** (6), 386.
[34] Grant, J.T. (2003) in *Surface analysis by Auger and X-Ray Photoelectron Spectroscopy*, edited by Briggs D. & Grant J.T. (IMPublications and SurfaceSpectra, Chichester, UK and Manchester, UK,).
[35] Childs, K.D., Vanier, L.A., Moulder, J.F., Paul, D.F., Stickle, W.F. & Watson, D.G. (1995) *Handbook of Auger Electron Spectroscopy*. (Physical Electronics, Eden Prairie, MN,).
[36] Powell, C.J., Erickson, N.E. & Madey, T.E. (1982) *Prog. Surf. Sci.* **25** (2-3), 87.
[37] Tilinin, I.S., Jablonski, A. & Werner, W.S.M. (1996) *Prog. Surf. Sci.* **52** (4), 193.
[38] Seah, M.P., Gilmore, I.S. & Spencer, S.J. (2001) *Surf. Interface Anal.* **31** (8), 778.
[39] Haas, T.W., Grant, J.T. & Dooley, G.J. (1972) *J. Appl. Phys.* **43** (4), 1853.
[40] Remaker, D.E. (2003) In *Surface Analysis by Auger and X-Ray Photoelectron Spectroscopy,* edited by D. Briggs and J. T. Grant (IMPublications and SurfaceSpectra, Chichester, UK and Manchester, UK,).
[41] Timmermans, B., Vaeck, N., Hubin, A. & Reniers, F. (2002) S*urf. Interface Anal.* **34** (1), 356.
[42] Ramaker D E. (1994) *J. Electron Spectrosc. Relat. Phenom.* **66** (3-4), 269.
[43] Zalar, A. (2000) *Inf. Midem-J. Microelectron. Electron. Compon. Mater.* **30** (4), 203.
[44] Hofmann, S. (2003) *Surf. Interface Anal.* **35** (7), 556.

[45] Derry, G.N. & Vanderlinde, W.E. (1992) *J. Vac. Sci. Technol. A-Vac. Surf. Films* **10** (4), 2826.
[46] Davidson, M.R., Hoflund, G.B. & Outlaw, R.A. (1991) *J. Vac. Sci. Technol. A-Vac. Surf. Films* **9** (3), 1344.
[47] Cao, Z.X. (2000) *Surf. Sci.* **452** (1-3), 220.
[48] Holloway, P.H. (1977) *Surf. Sci.* **66** (2), 479.
[49] Hofmann, S. (2005) *Appl. Surf. Sci.* **241** (1-2), 113.
[50] Inoue, M., Shimizu, R., Lee, H.I. & Kang, H.J. (2005) *Surf. Interface Anal.* **37** (2), 167.
[51] Mizuhara, Y., Bungo, T., Nagatomi, T. & Takai, Y. (2005) *Surf. Interface Anal.* **37** (3), 343.
[52] Zalar, A. (1985) *Thin Solid Films* **124** (3-4), 223.
[53] Paparazzo, E. (2003) *Archaeometry* **45** 615.
[54] Prutton, M. (2003) in *Surface Analysis by Auger and X-Ray Photoelectron Spectroscopy*, edited by D. Briggs & J.T. Grant (IMPublications and SurfaceSpectra, Chichester, UK and Manchester, UK).
[55] Jacka, M. (2001) *J. Electron Spectrosc. Relat. Phenom.* **114** 277.
[56] Ong J.L. & Lucas, L.C. (1998) *Biomaterials* **19** (4-5), 455.
[57] Rossi, A., Elsener, B., Hahner, G., Textor, M. & Spencer, N.D. (2000) *Surf. Interface Anal.* **29** (7), 460.
[58] Fan, H.Q. & Kim, H.E. (2002) *Japanese J. Appl. Phys.* **41** (11B), 6768.
[59] Matsumoto, K. (1998) *Scanning Microscopy* **12** (1), 61.
[60] Dittmar, K. (2004) *Surf. Interface Anal*. **36** (8), 837.
[61] Childs, K.D., Paul, D.F. & Schauer, S.N. (2001) *AIP Conference Proceedings* **550**, Characterization and metrology for ULSI technology, 312.
[62] Childs, K.D., Watson, D.G., Paul, D.F. & Clough, S.P. (1998) *AIP Conference Proceedings* **449**, Characterization and metrology for ULSI technology, 810.
[63] Childs, K.D., Paul, D.F. & Clough, S.P. (1996) *Proceedings Institute of Environmental Sciences* **42**, Contamination control; Symposium on minienvironments, 147.
[64] Fillmore, D.K. & Krasinski, H.A. (1998) *Surf. Interface Anal.* **26** (2), 109.
[65] Savage, R.N., (2003) *Solid State Technology* **46** (8), 57.
[66] Weightman, P. (2003) in *Surface analysis by Auger and photoelectron spectroscopy*, edited by D. Briggs & J. T. Grant (IMPublications and SurfaceSpectra, Chichester, UK and Manchester, UK,).
[67] Weiss, A., Mayer, R., Jibaly, M., Lei, C., Mehl, D. & Lynn, K.G. (1988) *Phys. Rev. Lett*. **61** (19), 2245.
[68] Fazleev, N.G., Kim, J., Fry, J.L. & Weiss, A.H. (2003) *Phys. Rev. B* **68** (24).
[69] Weiss, A.H., Yang, S., Zhou, H.Q., Jung, E. & Wheeler, S. (1995) *J. Electron Spectrosc. Relat. Phenom.* **72**, 305.
[70] Ohdaira, T., Suzuki, R., Mikado, T., Ohgaki, H., Chiwaki, M., Yamazaki, T. & Hasegawa, M. (1996) *Appl. Surf. Sci.* **101**, 73.
[71] Kim J.H. & Weiss, A.H. (2000) *Surf. Sci.* **460** (1-3), 129.
[72] Stefani, G., Gotter, R., Ruocca, A., Offi, F., Da Pieve, F., Iacobucci, S., Morgante, A., Verdini, A., Liscio, A., Yao, H. & Bartynski, R.A. (2004) *J. Electron Spectrosc. Relat. Phenom.* **141** (2-3), 149.
[73] Thurgate, S.M., Lund, C.P. & Wedding, A.B. (1994) *Nucl. Instrum. Methods Phys. Res. Sect. B—Beam interact. Mater. Atoms* **87** (1-4), 259.
[74] Robins, J.L. (1995) *Prog. Surf. Sci.* **48** (1-4), 167.
[75] Liscio, A., Gotter, R., Ruocco, A., Iacobucci, S., Danese, A.G., Bartynski, R.A. & Stefani, G. (2004) *J. Electron Spectrosc. Relat. Phenom.* **137-40**, 505.
[76] Werner, W.S.M., Smekal, W., Stori, H., Winter, H., Stefani, G., Ruocco, A., Offi, F., Gotter, R., Morgante, A. & Tommasini, F. (2005) *Phy. Rev. Lett*. **94** (3).